Determination of body waves quality factor in the NW Iran, with power spectrum analysis

Hooman Latifi[1], Reza Heidari[*1], Noorbakhsh Mirzaei[2]

1 Department of Earth Sciences, Science and Research Branch, Islamic Azad University, Tehran, Iran.
2 Department of Seismology, Institute of Geophysics, University of Tehran, Tehran, Iran.

Abstract
As one of the ways to identify seismological characteristics in the region, determining the quality factor of seismic mapping can provide valuable information about inside the earth. This study investigates local site effects as a function of frequency and presents a new relationship for determining the quality factor in northwestern Iran with regard to local site effects. These sites are selected so that their signal-to-noise ratio (SNR) is greater than 5. This study uses the Short-Time Fourier Transform (STFT) method in which a fixed time window and its multiplication by a given signal are used. The coefficients resulting from this transformation are considered as wave amplitudes at any frequency by performing a short-time Fourier transform. The amount of power spectrum decay is used instead of the ground displacement amplitude decay. Local site effects and kappa, a function of the path and site effects, were investigated and became the basis of spectral decay calculations. The results of this study were compared with those of the previous study based on conventional and classical methods and the accuracy of the methods was evaluated using standard deviation (SD) values. Finally, the quality factor equations were obtained for the North-South component $(N - S)$ as $Q(f) = (78 \pm 2)f^{(1.37\pm0.02)}$, for the East-West component (E-W) as $Q(f) = (62 \pm 2)f^{(1.5\pm0.03)}$, and for the vertical component (Z) as $Q(f) = (87 \pm 2)f^{(1.29\pm0.03)}$.
Keywords: Quality factor; Short-time Fourier transform; Power spectrum decay; Local site effects; Kappa factor.

1. Introduction
The amplitude range of seismic waves generally decreases as they pass through the earth due to two major factors, namely geometrical spreading and apparent attenuation of seismic waves. The geometrical spreading results in a decrease in signal energy due to the spherical geometric shape of the seismic wave propagation. Apparent attenuation is defined as a decrease in the amplitude range of seismic waves with an increase in hypocentral distance, due to the elastic and inelastic properties of the Earth's crust and upper mantle. In general, the overall attenuation of a seismic wave is expressed as the inverse quality factor Q and is a combination of internal attenuation and scattering. Quantitative investigation of the attenuation properties of seismic waves within the lithosphere is considered as an important parameter in seismic hazard assessment (Kumar et al. 2005).

Seismic wave attenuation has been suggested in many geophysical studies including strong ground motion simulation, physics-based seismic hazard assessment, ground thermal modeling, and ground thermal imaging (Jin and Aki 1988; Yoshimoto et al. 2015; Takemura et al. 2017). Wave attenuation is considered as one of the most important parameters in estimating seismic wave attenuation. The general attenuation mechanism is sensitive to changes in pressure and temperature, meaning that Q changes as a function of pressure and

----

*Corresponding author.
E-mail address (es): r.heidari@srbiau.ac.ir

temperature inside the Earth (Lay and Wallace 1995). Generally, at frequencies between 0.001 and 0.1 Hz, the Q parameter is essentially independent of frequency; however, it increases with an increase in frequency, for higher frequencies (Lay and Wallace 1995). Estimated values for Q are constant for frequencies less than 1 Hz and the relation dependent on Q frequency for frequencies higher than 1 Hz is as follows:

$$Q = Q_0 f^n \qquad (1)$$

Where n is a positive power and Q_0 is Q at the reference frequency, which is considered to be 1 Hz in this study. Here, f_0 is some reference frequency often taken to be 1 Hz. It has not been well considered for 1 Hz conventions. On ordinary regimens, 1 Hz has appeared predominance recommending comparable viability to high-frequency (HF). To address the aforementioned issues, we developed an accelerated low-frequency protocol applying 1 Hz.

Various studies have shown a direct relationship between Q_0 and regional tectonic activity such that the shear wave quality factor value at 1 Hz in stable tectonic regions is higher than that in active tectonic regions (Singh and Herrmann 1983). The reason is relatively high heat fluxes and higher uptake in active tectonic regions than in cooler stable (Lay and Wallace 1995). Heidari and Mirzaei (2017) determined that the shear wave attenuation relationship in this region as $Q(f) = (126)f^{(0.73)}$ using a continuous wavelet transform. Furthermore, Motazedian (2006) determined the shear wave attenuation relationship for the northern region of Iran as $Q(f) = (87)f^{(1.46)}$. In general, there are various methods for estimating the quality factor of seismic waves, some of which are more sensitive and some less sensitive to

changes in attenuation. In recent years, these methods are used to explore attenuation properties of earth in the world (Liang et al. 2014; Lin 2014; Kumar et al. 2016; Bora and Biswas 2017; De Siena et al. 2017).

Recently, the seismic wave's attenuation in different parts of Iran plateau and using different approaches are reported (e.g., Mahood and Hamzehloo 2011; Farrokhi et al. 2015; Irandoust et al. 2016; Farrokhi and Hamzehloo 2017; Heidari and Mirzaei 2017; Amiri Fard et al. 2019; Fard et al. 2020). Common methods of determining the quality factor are divided into three main categories. The first category is based on the coda-normalization to estimate the attenuation of Q_p^{-1} and Q_s^{-1} body waves still used today by various researchers worldwide (Aki 1980). The second category is the use of the body wave spectral decay method. This category uses spectral amplitude ratios, at least for the two distances traveled by the waves. The third category is estimation using the single backscattering method to estimate the attenuation of coda waves (Aki and Chouet 1975). Therefore, different approaches lead to different results. This study has proposed a method for determining Q based on the wave spectral decay rate referred to as the power spectrum. The proposed method uses signal data at multiple points in the time and frequency range to estimate the energy loss of the waves without the need for a source wave spectrum. When the power spectrum method is used to estimate the presence of correlations in real nonstationary time series, as in the case of heartbeat interval signals, it may lead to unreliable results. In past decades, alternative methods have been proposed to the assessment of correlations for stationary and nonstationary time series. A method which is very appropriate to the assessment of correlations in stationary and nonstationary time series is the disceate Fourier analyse.

This method was introduced to quantify long-range correlations in the heartbeat interval time series and DNA sequences. Since the study area is highly populated and industrial, engineering seismic studies will be inevitable in order to gain a better understanding of the key parameters in the area.

2. Tectonic setting
Northwestern Iran is tectonically and seismically active, an area that has experienced several major earthquakes. The area has witnessed many historical and instrumental earthquakes. As an example, two major devastating earthquakes of Ahar-Varzaghan in 2012, with magnitudes of ٦٫٤ and ٦٫٥, are the latest seismic events in the region to occur with a time difference of 11 minutes. Fig 1 shows the epicenter location and focal

mechanism of these two earthquakes. In the study area, the depth of earthquakes are mainly in the range of 10-20 km and their magnitude are up to 6.5. Tabriz, located in the northwestern part of Iran as one of the major metropolises, is located in an earthquake-prone region and has experienced several devastating earthquakes throughout history. For example, the 1721 magnitude 7.7 earthquakes ruptured the southeastern segment of the Tabriz Fault, and the 1780 earthquake of magnitude 7.7, which was the largest historical earthquake in the city, ruptured its northwestern segment. The focal mechanisms of earthquakes indicate that the convergence between the Arabian and Eurasian plates in this region is offset by dextral strike-slip faults (Jackson 1992).

The North Tabriz Fault (NFT) is considered as one of the major active faults of northwestern Iran which has a visible surface outcrop. This fault has an approximate northwest-southeast trend and a length of approximately 150 km (Hessami et al. 2003) The slip rate across this fault has been suggested at least 2 mm/year (Karakhanian et al. 2004). Hessami et al. (2003) have proposed dextral strike-slip displacement of this fault at 7 ± 1 mm/year, which corresponds to 8 ± 2 mm/year for Vernant et al.'s (2004) study. Alongside numerous active faults, other important structural features of the area include the Sahand and Sabalan volcanoes (Fig 1). Bavali et al. (2016) showed that the presence of these two volcanoes caused a thermal anomaly beneath them. The presence of thermal anomaly has caused a decrease in seismic wave velocity as well as a decrease in attenuation in this region.

3. Data
The study area is an area between 39-34° north latitude and 52-44° east longitude. This study used an average of 2580 earthquakes with magnitude 2.5-6.5, recorded in 2006-2016 at the IRSC of the Institute of Geophysics, University of Tehran. These waveforms are selected so that their SNR is greater than 5, which is qualitatively appropriate. The studied frequency range is 1-8 Hz. Eearthquake engineers are interested in this frequency range.

Since the general form of the equation will eventually be presented in $Q = Q_0 f^n$ power form, frequencies of 1-8 Hz are considered. This study used sites from 14 seismograph stations of the Iran. Fig 1 shows the location of seismograph stations and the epicenter of earthquakes in the study area. Moreover, Fig 2 presents the statistics associated with the frequency of earthquakes in different magnitude intervals in northwestern Iran. This figure presents an overview of the earthquakes in the magnitude interval studied (i.e., 2.5-6.5).
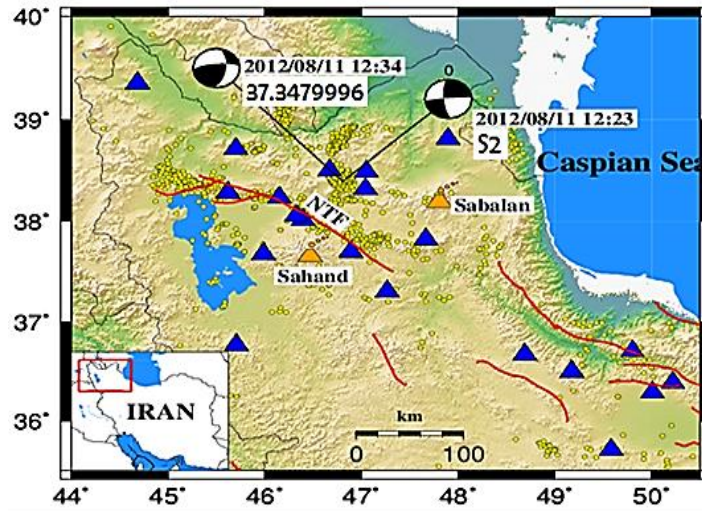
Fig 1. Study area, seismograph stations, the epicenter of earthquakes of magnitude 2.5-6.5 in 2006-2016 (Official Website of Iranian Seismological Center (IRSC), Institute of Geophysics, University of Tehran).
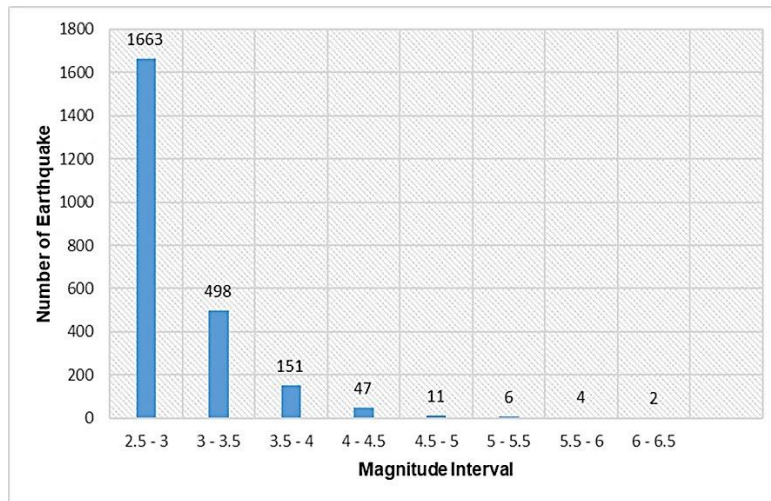

Fig 2. Magnitude-Frequency Diagram for the Earthquakes in Northwestern Iran (2006-2016).

4. Theory and Methodology

The quality factor obtained by the various methods is an overall and apparent Q which includes other attenuating mechanisms such as geometric distribution, reflection or scattering, as well as non-elastic absorption. The overall Q is related to the intrinsic Q and the Q resulting from scattering by the following equation (Spencer et al. 1982):

$$\frac{1}{Q_{eff}} = \frac{1}{Q_{int}} + \frac{1}{Q_{add}} \qquad (2)$$

Some of the effects of scattering can be separated by different methods. However, in the general case, it is impossible to control all these effects and the result is an apparent Q. Some mathematical methods of calculating the quality factor are more sensitive to these scattering effects and some are less sensitive. Thus, this is one of the reasons that different methods yield different results. The energy of the body waves decreases at the frequency f exponentially with an increase in the distance r following Equation $e^{-\pi r f Q_p^{-1}/\alpha_0} e^{-\pi r f Q_p^{-1}/\alpha_0}$ for P waves and Equation $e^{-\pi r f Q_s^{-1}/\beta_0} e^{-\pi r f Q_s^{-1}/\beta_0}$ for S waves. A geometric distribution coefficient r is introduced for P and S waves for the spherical geometric distribution of the waves in a 3D homogeneous velocity structure. Hence, the spectral amplitude of the waves will follow the following equations as UP and US (Fehler et al. 1992).

$$U_{(r,f)}^{P} \propto \frac{e^{-\frac{\pi r f Q_p^{-1}}{\alpha_0}}}{r} \qquad (3)$$

$$U_{(r,f)}^{S} \propto \frac{e^{-\frac{\pi r f Q_S^{-1}}{\beta_0}}}{r} \qquad (4)$$

where Q is the quality factor, f is the frequency, and r is the distance traveled; α_0 and β_0 are the velocities of the waves P and S, respectively. In this study, the body waves can be described as modified by (Benz et al. 1997) for frequency-dependent Q estimation.

The observed magnitude of the amplitude of body waves (A) recorded at frequency f for each earthquake at each station can be modeled using Eq. 5 (McNamara 2000).

where Q is the quality factor, f is the frequency, and r is the distance traveled; ; α_0 and β_0 are the velocities of the waves P and S, respectively. In this study, the body waves can be described as modified by (Benz et al. 1997) for frequency-dependent Q estimation. The observed magnitude of the amplitude of body waves (A) recorded at frequency f for each earthquake at each station can be modeled using Eq. 5 (McNamara 2000)

$$A(f) = R^{-\gamma} S(f) G(f) \exp(-\pi f R/Q\beta) \qquad (5)$$

where S(f) is the source spectrum, G(f) is the magnification at the site, R is the distance of earthquake epicenter to the station, γ is the geometric propagation power, Q is the quality factor of the body waves at frequency f, and β is the average velocity of the body wave in the crust. By taking the natural logarithm of Eq. 4, we will have Eq. 6 (McNamara 2000):

$$\ln A(f) + \gamma \ln R = A - (\pi f/Q\beta) R \qquad (6)$$

According to Eq. 6, the slope of the best-fit line using the linear least-squares ln A(f) + γ ln R in R corresponds to $-\pi f/Q\beta$.

Furthermore, quality factors are estimated for several simulated scenarios with specified values of Q(f). This study examines the soil layers in a given site and the motion of the earth's surface and compares changes in the amplitude and frequency of bedrock movement in different states.

Although these changes are considered as part of the path effect, the local conditions of the site are considered independent of the distance between the source and the site. In general, the overall effect of the site S(f) is expressed as the product of "reinforcement by the near-surface site B(f) by the "near-surface (upper-crust) attenuation" commonly used as exp(πfκ0) (Boore 2003):

$$S(f) = B(f)e^{-\pi f k_0} \qquad (7)$$

Due to the lack of appropriate information on soil classification at the stations used in this study, the reinforcement of site B(f) has been replaced with the horizontal-to-vertical (H/V) spectral ratio, which is known as an approximate estimate of the reinforcement at the site (Motazedian 2006).

In Eq. 7. κ0 denotes near-surface attenuation and is related to the kappa factor as follows (Anderson and Quaas 1988).

$$k = k_0 + k_r R \qquad (8)$$

	A	B	C	D	E	F	G	H	I	J
1	Weighted Kappa									
2										
3	Observations									
4										
5			Questionnaire						Weights	
6	Interview	Often	Seldom	Never	Total			Often	Seldom	Never
7	Often	16	6	2	24		Often	0	1	2
8	Seldom	4	10	1	15		Seldom	1	0	1
9	Never	3	0	8	11		Never	2	1	0
10	Total	23	16	11	50					
11										
12	Expectations									
13										
14			Questionnaire							
15	Interview	Often	Seldom	Never	Total		Kappa	0.500951		
16	Often	11.04	7.68	5.28	24					
17	Seldom	6.9	4.8	3.3	15					
18	Never	5.06	3.52	2.42	11					
19	Total	23	16	11	50					
20										

Table 1. The results of calculated kappa values in this study.

The parameter κ for the horizontal and vertical components is obtained from the slope of the logarithmic amplitudes of the Fourier spectrum in the frequency band to be determined at those spectral amplitudes by frequency. In this general case, part of the value of $\kappa_0 (\Delta\kappa_0 = \kappa_{0h} - \kappa_{0v})$ already contains the H/V ratio;

therefore, we have to subtract it from the near-surface attenuation value associated with the horizontal component (Table 1). Hence, the term "site for the horizontal component" can be considered as follows (Motazedian 2006):

$$s(f) = \frac{H}{V} e^{-\pi(K_{0h} - \Delta H_0)f} = \frac{H}{V} e^{-\pi K_{0v} f} \qquad (9)$$

We will try several methods to calculate H/V ratios including averaging, linear, and quadratic regression ratios. The results show that the "H/V ratio averaging" case, including all frequency content, partially minimizes the average residual errors for the source function that we were eventually searching for the earthquakes that occurred in this region. Therefore, the effect of the site is written as follows:

$$S_{ij}(f) = \left(\overline{H/V}\right)_{ij} e^{-\pi k_{0v}f} \qquad (10)$$

Where $\left(\overline{H/V}\right)_{ij}$ is the average H/V ratio of the earthquake i recorded at station j.

Kappa factors for both vertical and horizontal components are obtained from the slope of the acceleration spectrum amplitude at higher frequencies. Due to the lack of sufficient information on soil classification for the stations used in this study, the H/V spectral ratio was used as an alternative to an approximate estimate of site reinforcement. As Motazedian (2006) put it, the general term "site", the product of site reinforcement multiplied by near-surface attenuation, is obtained by Equation $(H/v)\, e^{-nkf}$

The amplitude range of seismic waves in a given radius around the earthquake's epicenter is not similar and depends on the azimuth of the station and fault strike, the mechanism, and the effect of directivity. In almost all amplitude decay studies, these effects are forcibly discarded as random changes despite the use of large earthquakes.

The earthquakes recorded in the area with an acceptable azimuthal gap are used to solve this problem. Higher volumes of data and more homogeneous coverage of the study area with small seismic waves significantly reduce the effect of radiation pattern and directivity. The largest azimuthal gap between azimuthally adjacent stations (in degrees).

Boore (2003) showed that the maximum amount of mapping amplitude in a site strongly depends on the characteristics of the area near the source and the station. Additionally, slight changes in azimuth will affect the wave amplitude decay, as it results in large changes in the beam path in a 3D heterogeneous environment. This uncertainty in amplitude determination can make it 10 times more or less. Thus, providing a moderate attenuation relationship for the entire region requires the use of numerous earthquake sources and receivers such that the effects of the sources and receivers are reduced by averaging and an acceptable value is obtained for the energy-loss function (ELF) in the area. In the northwestern region of Iran, the number of large earthquakes in the instrumental period (i.e., post-1900) is very limited and is restricted to a few 6.5-magnitude earthquakes such as the Ahar-Varzaghan twin earthquakes. The attenuation parameters obtained from this study can be strongly influenced by the faulting mechanism and regional geology in the direction of earthquake beams. In most attenuation studies, these effects have been ignored as random variations despite

the use of large earthquakes. In addition, it has been shown empirically that there is an inverse relationship between magnitude and amplitude decay in the far-field, with the amplitude decay decreasing with an increase in magnitude.

As the investigation of the wave amplitudes is used to study the non-elastic behavior of the environment, these amplitudes depend on the earthquake source, which is not precisely known, as well as on the elastic and non-elastic effects of the environment traveled by the wave from the source to the receiver. Hence, this study investigated the quality factor for both environmental and site effects (Table 2). In other words, the attenuation relationship provides a fundamental relationship between earthquake characteristics such as response spectrum and various parameters such as magnitude, soil conditions, and site-to-source distance.

Table 2. Frequency statistics of earthquakes in different large periods in the northwestern region of Iran from 2006 to 2016 (Website of the National Seismological Center)

No	Magnitude range	Number of available data
1	2.5-3	1663
2	3-3.5	498
3	3.5-4	151
4	4-4.5	47
5	4.5-5	11
6	5-5.5	6
7	5.5-6	4
8	6-6.5	2

5. Calculations and Results

Generally, the Q values are obtained from the waves based on changes in certain properties. This study used the relative power spectrum decay method, time-domain data, and multi-point signal data to estimate the quality factor as well as to avoid local interference. In this study, a high-resolution technique with is used to estimate wave attenuation. The local effects of the site and kappa, which are functions of the effect of the path and the site, will be examined and will be the basis for spectral decay alculations. Finally, the calculated values are compared with other results of attenuation measurements in the study area obtained using previous conventional and classical methods and the accuracy of the methods evaluated using the standard deviation and also compared with other relationships obtained from the area. The case study will be reviewed. The wave spectral energy is represented by E and defined as an integral over the power spectrum frequency range (i.e., squared amplitude spectrum). The pre-attenuation wave spectrum energy equals Es and the post-attenuation wave spectrum energy equals ER. According to Eq. 6, it is assumed that the attenuation is frequency-dependent and all the effects of the site, such as kappa and $e^{-\pi kf}$ which are frequency-dependent, are considered in the local effects of the station $(G(f))$ while computing, while the effects of the site can strengthen or weaken the domain itself that are

unfortunately not applied in this equation. Therefore, in this study, we attempted to calculate the extent of site effects on attenuation relationships more accurately by examining wave amplitude before and after attenuation using the power spectrum. First, we calculate the local effect of the site including kappa and H/V ratios on the stations studied, as follows.

- Pre-attenuation wave amplitude relationship (Benz et al. 1997):

$$A = S(f)G(f) \qquad (11)$$

- Post-attenuation wave amplitude relationship (Benz et al. 1997):

$$A' = S(f)G(f)e^{-k\pi f}r^{-\gamma}e^{-\pi fR/Q\beta} \qquad (12)$$

- Now, using the energy spectrum equation, we will have:

$$E = 1/N \sum_{i=1}^{N} a_i^2 \qquad (13)$$

- Considering the pre-attenuation (E) and post-attenuation (E') energy spectrum, we will have:

$$\frac{E'}{E} = \frac{S^2 G^2 e^{-2k\pi f}r^{-2\gamma}e^{-2\pi fR/Q\beta}}{S^2 G^2} \qquad (14)$$

$$\frac{E'}{E} = \left(e^{-\pi kf}r^{-\gamma}e^{-\pi fR/QB}\right)^2 \qquad (15)$$

Since it is not possible to analyze and determine the energy spectrum due to the inability to detect specific frequencies along the path, using the power spectrum in direct relation to energy, we will have:

$$LN\left(\frac{E'/N}{E/N}\right) = 2LN\left(e^{-\pi kf}r^{-\gamma}e^{-\pi fR/Q\beta}\right) \qquad (16)$$

Finally, we can fully characterize $H/\ ve^{-nkf}$ effects in local site effects.

The main step, according to the distribution of accelerometers and seismic stations due to the need for different frequency spectrum, we collected all the data in the study area. In this regard, S and P-waves are used in order to estimate the attenuation values of the study arae. This will increase the accuracy of the calculation of the attenuation parameter at different stations with respect to the site effects, which is different from previous methods that specifying the local effects of the station and kappa by using the short-time Fourier transform method to apply the power spectrum instead of the wave amplitude. Fourier transform clearly reveals the frequency of a stable or non-stable signal, but it cannot detect the time of the occurrence of that frequency. In order to solve this problem in non-stable systems, the STFT algorithm (Gabor 1946) was used. In this method, the signal was divided into separate stable signals using a window function. Over the past several decades, various types of window functions have been developed on the different type of seismic waves.

In this study, the Hamming window was applied for data processing. This choice is very close to that which minimizes peak side-lobe level- the lowest possible within the generalized Hamming family. Moreover, in order to study the amplitude decay with time in certain frequency ranges as another approach, short time Fourier transform (STFT) has been used to separate different composed signals of an earthquake waveform in time-frequency domain (Vernosfaderani et al. 2019).

Note that the integration intervals will be finite if the wave energy ratio in the frequency range is calculated. According to Parseval's Theorem in the Fourier transform method, one can also estimate the energy ratio in the time domain, i.e., the sum of the quadratic values of the periodic data. Thus, this study determined that the "energy ratio" method can be used to derive Q values in the time and frequency range and waveform spectral decay analysis was ignored. Ultimately, we obtain an optimized equation based on the relation of Benz et al. (1997).In this study, the computational results along with the comparison between Fast Fourier Transform (FFT) and STFT are presented graphically.

Because Fourier transforms determines the frequency content of the signal; in cases where frequency behavior is important, it is especially important. For all its ability to convert to Fourier transform, it has the fundamental disadvantage that in the frequency domain, the time information of the signal will not be accessible. To compensate for this shortcoming in the Fourier transform, a short-time Fourier transform was introduced, in which we apply the Fourier transform to a signal in a short time window, thus converting the signal from a one-dimensional time basis to a two-dimensional time-frequency basis.

Similar to the Fourier transform introduced (Gabor 1946), the short-time Fourier transform was used to analyze only a small portion of a signal at a time, a technique called signal windowing.

The Gabor method is called the Fourier transform for short time (STFT). The values of the seismic wave quality coefficient were calculated without considering the Kappa coefficient. Fig 3 shows Frequency-Apparent Quality Factor Diagram by the Fourier Transform Method and Short-Time Fourier Transform without Considering Kappa Factor for Z component.

Fig 4 shows Frequency-Apparent Quality Factor Diagram by the Fourier Transform Method and Short-Time Fourier Transform Without Considering Kappa Factor for E component and Fig 5 shows Frequency-Apparent Quality Factor Diagram by the Fourier Transform Method and Short-Time Fourier Transform Without Considering Kappa Factor for N component.

6. Discussion

The accuracy of the methods was evaluated using standard deviation as well as comparison with other equations obtained from the study area.

Boore (2004) showed that the maximum amplitude of the waveform in a place depends strongly on the characteristics of the area near the source and the station. The amount of attenuation will affect the amplitude of the wave, which can increase or decrease the amplitude by up to 10 times, so providing a moderate attenuation relationship for the whole area requires the use of abundant seismic sources and many stations. By averaging, the effects of amplitude od waves on the

source and receiver are reduced to an acceptable value for the energy drop function in the area.

The quality factor equation was obtained for the North-South horizontal component (N-S) as $Q(f)=(78\pm2)f^{(1.37\pm0.02)}$ (Fig 6), for the East-West horizontal component (E-W) as $Q(f)=(62\pm2)f^{(1.5\pm0.03)}$ (Fig 7), and finally, for the vertical component (Z) as $Q(f)=(87\pm2)f^{(1.29\pm0.03)}$ (Fig 8). This study thoroughly examined local site effects and kappa, a function of the path and site, which are the basis for the spectral decay calculations.
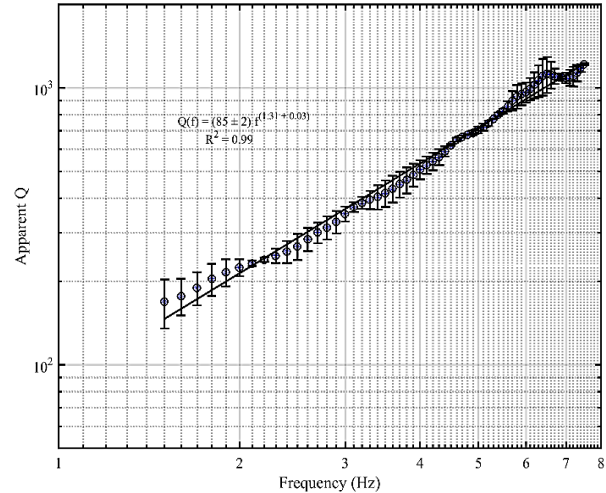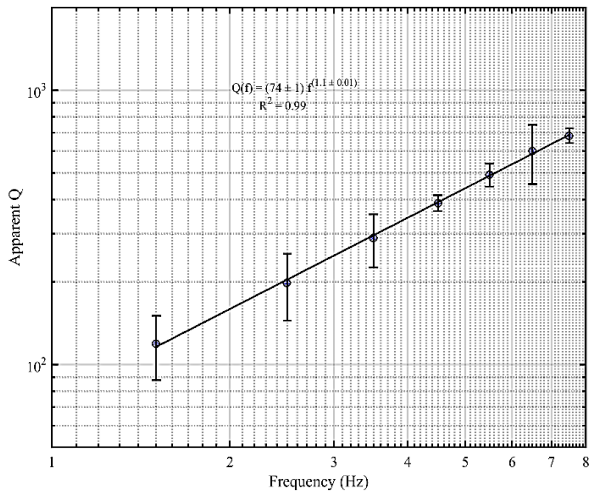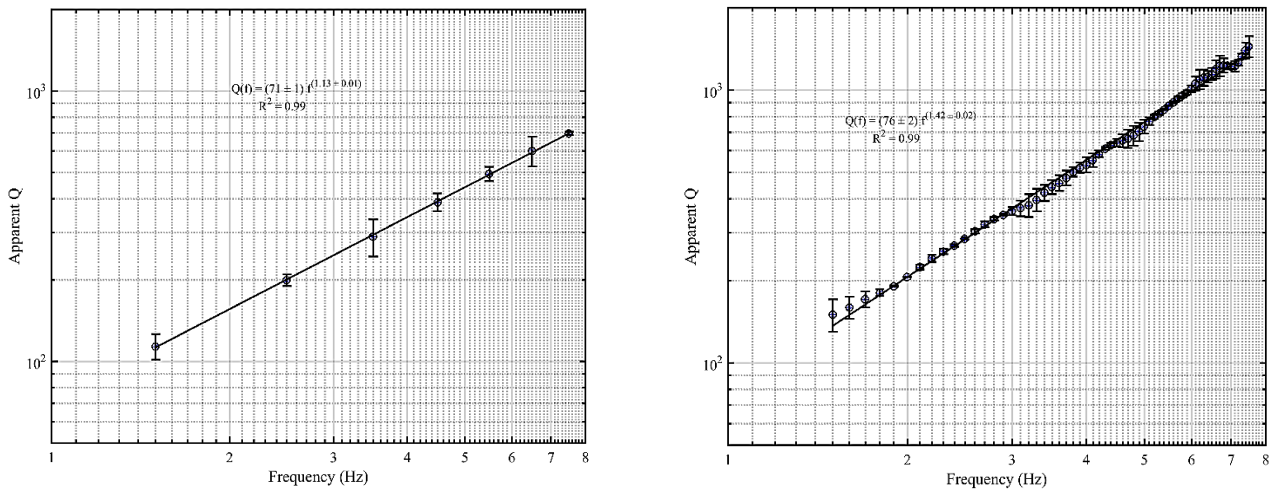

Fig 3. Frequency-Apparent Quality Factor Diagram by the Fourier Transform Method Without Considering Kappa Factor for Z component (left), and frequency-Apparent Quality Factor Diagram by Short-Time Fourier Transform Without Kappa Factor (right).
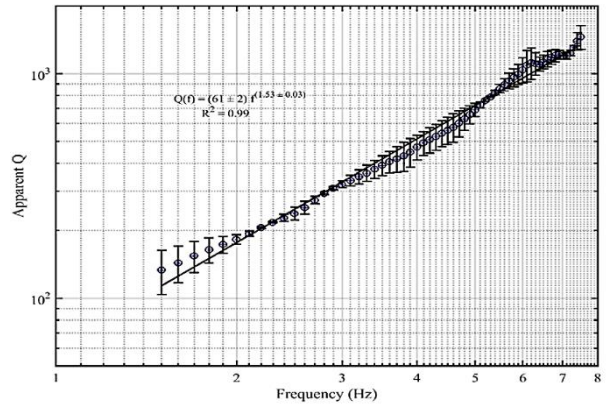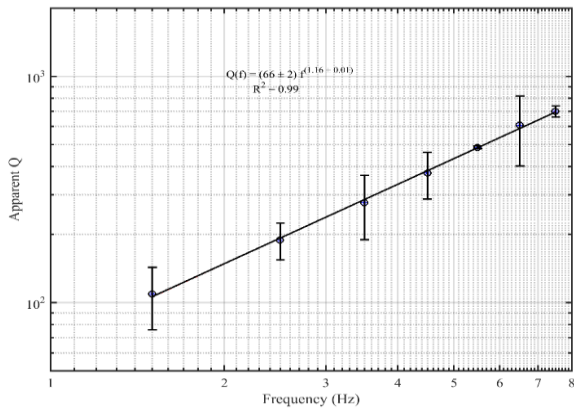
Fig 4. Frequency-Apparent Quality Factor Diagram by the Fourier Transform Method Without Considering Kappa Factor for E component (left), and Frequency-Apparent Quality Factor Diagram by the Short-Time Fourier Transform Without Kappa Factor (right).

Fig 5. Frequency-Apparent Quality Factor Diagram by the Fourier Transform Method Without Considering Kappa Factor for N Component (left), and Frequency-Apparent Quality Factor Diagram by the Short-Time Fourier Transform Method Without Considering Kappa Factor (right).
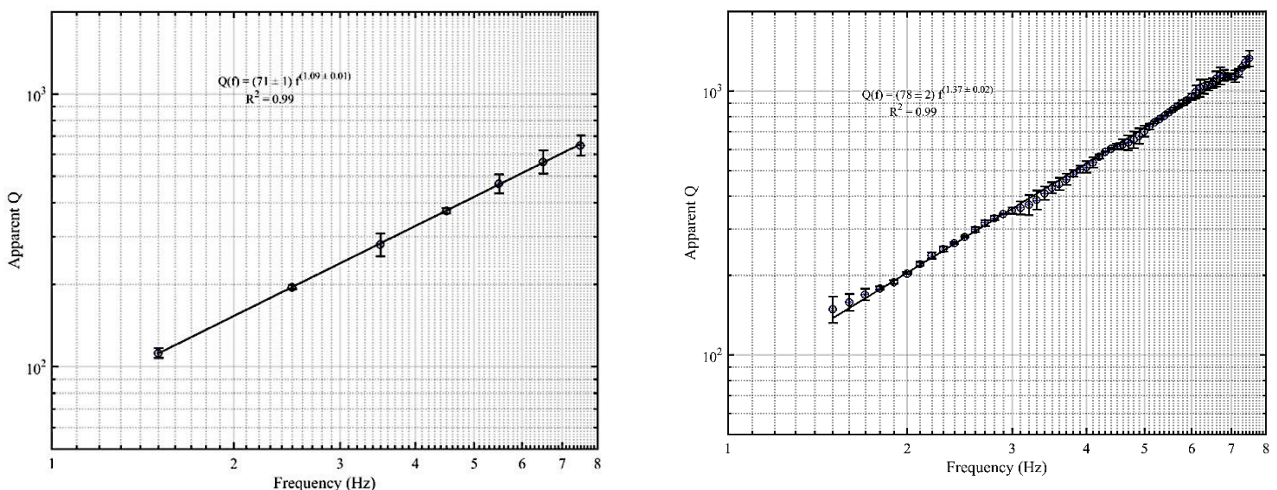

Fig 6. Frequency-Apparent Quality Factor Diagram by the Fourier Transform Method Considering Kappa Factor for N Component (left), and Frequency-Apparent Quality Factor Diagram by the Short-Time Fourier Transform Method Considering Kappa Factor (right).

Furthermore, the parameter Q was determined for the northwestern region of Iran using the Short-Time Fourier Transform (STFT) method and the attenuation was presented using the quality factor. It was found that the STFT model can be used as a tool at the appropriate time-frequency (Fig 9).

Due to the low values and high absorption of shear and P waves in northwestern Iran, the amplitude range of seismic waves is greatly reduced while crossing the earth, which was consistent with our studies. This effect of seismic wave absorption will cause a reduction in earthquake damage at appropriate distances from faults at the time of the earthquake. In fact, seismic attention indicates the deflection of the waves or the reorientation of the radiated energy due to the existence of inhomogeneities in the earth and causes the energy of the seismic waves to expand again due to the collision of the waves with the heterogeneities of the environment.
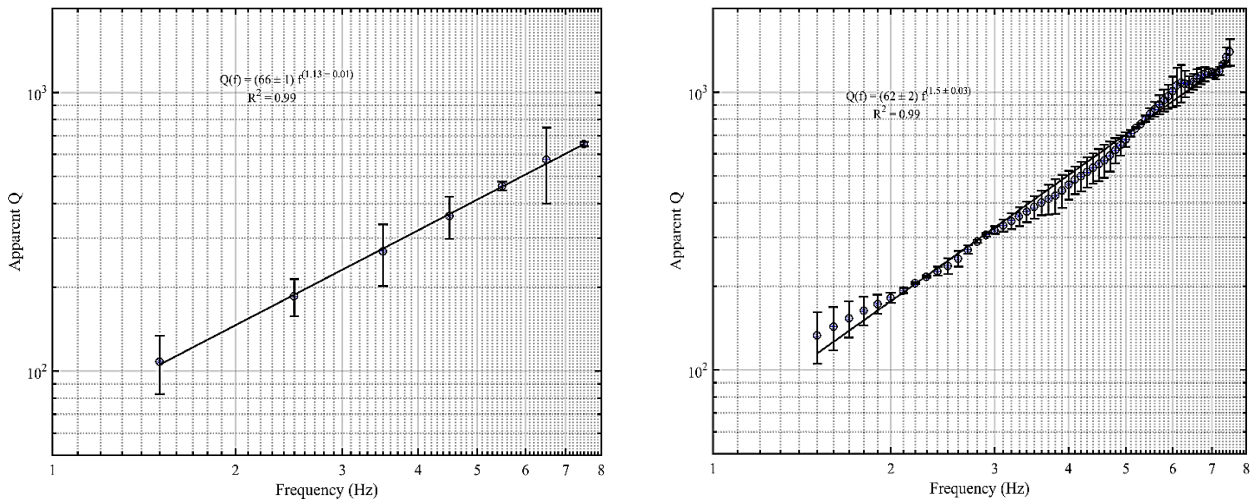
Fig 7. Frequency-Apparent Quality Factor Diagram by the Fourier Transform Method Considering Kappa Factor for E Component (left), and Frequency-Apparent Quality Factor Diagram by the Short-Time Fourier Transform Method Considering Kappa Factor (right).
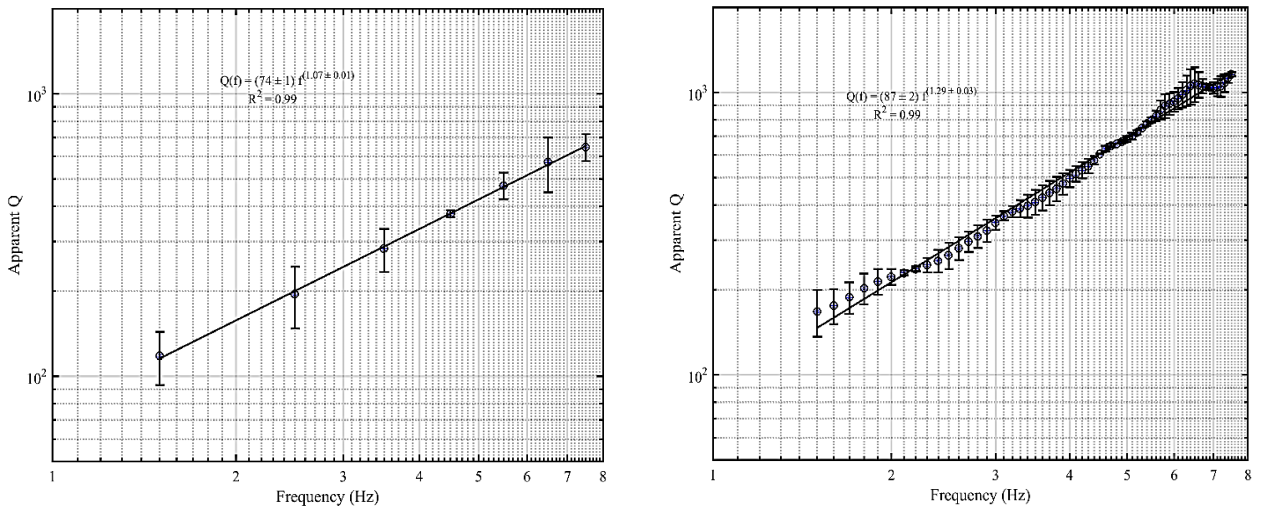

Fig 8. Frequency-Apparent Quality Factor Diagram by the Fourier Transform Method Considering Kappa Factor for Z component (left), and frequency-Apparent Quality Factor Diagram by the Short-Time Fourier Transform Method Considering Kappa Factor (right).
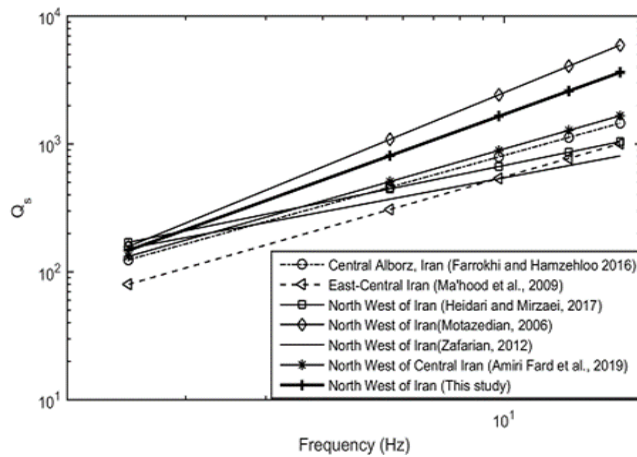

Fig 9. A comparison between the quality factors obtained in this study and the values obtained for other individuals in the region.

7. Conclusion

This study used a high-resolution technique to estimate the attenuation of S and surface waves. Local site effects and kappa, a function of the path and site, were investigated and became the basis for the spectral decay calculations. One of the aims of this study was to present a high-resolution technique for estimating apparent attenuation, i.e., a combination of intrinsic attenuation and geometrical spreading. Moreover, the calculated values in this study were compared with other attenuation measurement results obtained in the study area using the previous conventional and classical methods, employing the power spectrum decay method along with a short-time Fourier transform. The results of this study were compared with those of the previous works based on conventional and classical methods and the accuracy of the methods was evaluated using standard deviation (SD) values. Finally, the quality factor equations were obtained for the North-South component $(N-S)$ as $Q(f) = (78 \pm 2)f^{(1.37 \pm 0.02)}$ for the East-West component (E-W) as $Q(f) = (62 \pm 2)f^{(1.5 \pm 0.03)}$ and for the vertical component (Z) as $Q(f) = (87 \pm 2)f^{(1.29 \pm 0.03)}$

Acknowledgments

References

Aki K (1980) Attenuation of shear-waves in the lithosphere for frequencies from 0.05 to 25 Hz, *Physics of the Earth and Planetary Interiors* 21:50-60.

Aki K, Chouet B (1975) Origin of coda waves: source, attenuation, and scattering effects, *Journal of geophysical research* 80:3322-3342.

Amiri Fard R, Javan Doloei G, Rahimi H, Farrokhi M (2019) Attenuation of P and S waves in Western part of Iran, *Geophysical Journal International* 218:1143-1156.

Anderson J, Quaas R (1988) The Mexico earthquake of September 19, 1985—Effect of magnitude on the character of strong ground motion: An example from the Guerrero, Mexico strong motion network, *Earthquake Spectra* 4:635-646.

Bavali K, Motaghi K, Sobouti F, Ghods A, Abbasi M, Priestley K, Mortezanejad G, Rezaeian M (2016) Lithospheric structure beneath NW Iran using regional and teleseismic travel-time tomography, *Physics of the Earth and Planetary Interiors* 253:97-107.

Benz HM, Frankel A, Boore DM (1997) Regional Lg attenuation for the continental United States, *Bulletin of the Seismological Society of America* 87:606-619.

Boore DM (2003) Simulation of ground motion using the stochastic method, *Pure and applied geophysics* 160:635-676.

Boore DM (2004), "Long-period ground motions from digital acceleration recordings: a new era in engineering seismology", *Proceedings of the International Workshop on Future Directions in Instrumentation for Strong Motion and Engineering Seismology*. Kluwer: Kusadasi, Turkey. Bora N, Biswas R (2017) Quantifying regional body wave attenuation in a seismic prone zone of northeast India, *Pure and Applied Geophysics* 174:1953-1963.

Bora N, Biswas R (2017) Quantifying Regional Body Wave Attenuation in a Seismic Prone Zone of Northeast India, *Pure and Applied Geophysics* 174: 1953-1963.

De Siena L, Amoruso A, Pezzo ED, Wakeford Z, Castellano M, Crescentini L (2017) Space-weighted seismic attenuation mapping of the aseismic source of Campi Flegrei 1983–1984 unrest, *Geophysical Research Letters* 44:1740-1748.

Fard RA, Javan-Doloei G, Farrokhi M, Rahimi H, Mahood M (2020) Coda wave attenuation's dependency on Lapse time and frequency in west of Iran plateau using local earthquakes, *Annals of Geophysics* 63:437.

Farrokhi M, Hamzehloo H (2017) Body wave attenuation characteristics in the crust of Alborz region and North Central Iran, *Journal of Seismology* 21:631-646.

Farrokhi M, Hamzehloo H, Rahimi H, Allamehzadeh M (2015) Estimation of coda-wave attenuation in the central and eastern Alborz, Iran, *Bulletin of the Seismological Society of America* 105:1756-1767.

Fehler M, Hoshiba M, Sato H, Obara K (1992) Separation of scattering and intrinsic attenuation for the Kanto-Tokai region, Japan, using measurements of S-wave energy versus hypocentral distance, *Geophysical Journal International* 108:787-800.

Gabor D (1946) Theory of communication. Part 1: The analysis of information, Journal of the Institution of Electrical Engineers-Part III: *Radio and Communication Engineering* 93:429-441.

Heidari R, Mirzaei N (2017) Region-specific S-wave attenuation for earthquakes in northwestern Iran, *Journal of Seismology* 21:1335-1344.

Hessami K, Jamali F, Tabassi H (2003) Major active faults of Iran, IIEES, Tehran.

Irandoust MA, Sobouti F, Rahimi H (2016) Lateral and depth variations of coda Q in the Zagros region of Iran, *Journal of Seismology* 20:197-211.

Jackson J (1992) Partitioning of strike-slip and convergent motion between Eurasia and Arabia in eastern Turkey and the Caucasus, Journal of Geophysical Research: *Solid Earth* 97:12471-12479.

Jin A, Aki K (1988) Spatial and temporal correlation between coda Q and seismicity in China, *Bulletin of the Seismological Society of America* 78:741-769.

Karakhanian AS, Trifonov VG, Philip H, Avagyan A, Hessami K, Jamali F, Bayraktutan MS, Bagdassarian H, Arakelian S, Davtian V (2004) Active faulting and

natural hazards in Armenia, eastern Turkey and northwestern Iran, *Tectonophysics* 380:189-219.

Kumar N, Parvez IA, Virk H (2005) Estimation of coda wave attenuation for NW Himalayan region using local earthquakes, *Physics of the earth and planetary interiors* 151:243-258.

Kumar R, Gupta S, Singh S, Kumar A (2016) The Attenuation of High-Frequency Seismic Waves in the Lower Siang Region of Arunachal Himalaya: Q α, Q β, Q c, Q i, and Q s, *Bulletin of the Seismological Society of America* 106:1407-1422.

Lay T, Wallace T (1995) Modern global seismology. Academic, Inc San Diego, CA.

Liang X, Sandvol E, Kay S, Heit B, Yuan X, Mulcahy P, Chen C, Brown L, Comte D, Alvarado P (2014) Delamination of southern Puna lithosphere revealed by body wave attenuation tomography, Journal of Geophysical Research: *Solid Earth* 119:549-566.

Lin G (2014) Three-dimensional compressional wave attenuation tomography for the crust and uppermost mantle of northern and central California, Journal of Geophysical Research: *Solid Earth* 119:3462-3477.

Mahood M, Hamzehloo H (2011) Variation of intrinsic and scattering attenuation of seismic waves with depth in the Bam region, East-Central Iran*, Soil Dynamics and Earthquake Engineering* 31:1338-1346.

McNamara D (2000) Frequency dependent Lg attenuation in south-central Alaska, *Geophysical research letters* 27:3949-3952.

Motazedian D (2006) Region-specific key seismic parameters for earthquakes in northern Iran, *Bulletin of the Seismological Society of America* 96:1383-1395.

Riaz MS, Bin S, Naeem S, Kai W, Xie Z, Gilani SM, Ashraf U. (2019) Over 100 years of faults interaction, stress accumulation, and creeping implications, on Chaman Fault System, *Pakistan. International Journal of Earth Sciences* 108(4):1351-1359.

Singh S, Herrmann RB (1983) Regionalization of crustal coda Q in the continental United States, Journal of Geophysical Research: *Solid Earth* 88:527-538.

Spencer T, Sonnad J, Butler T (1982) Seismic Q-Stratigraphy or dissipation, *Geophysics* 47:16-24.

Takemura S, Kobayashi M, Yoshimoto K (2017) High-frequency seismic wave propagation within the heterogeneous crust: effects of seismic scattering and intrinsic attenuation on ground motion modelling, *Geophysical Journal International* 210:1806-1822.

Vernant P, Nilforoushan F, Chery J, Bayer R, Djamour Y, Masson F, Nankali H, Ritz J-F, Sedighi M, Tavakoli F (2004) Deciphering oblique shortening of central Alborz in Iran using geodetic data, *Earth and Planetary Science Letters* 223:177-185.

Vernosfaderani SLJ, Heidari R, Mirzaei N, Rahimi H, Meshinchi-Asl M (2019) Coda wave attenuation in the northwestern Iran, using short time Fourier transform, *Journal of Seismology* 23:1085-1095.

Yoshimoto K, Takemura S, Kobayashi M (2015) Application of scattering theory to P-wave amplitude fluctuations in the crust, Earth, *Planets and Space* 67:199.